Honeycomb structures on Ge(111): A structure-factor analysis

Patrici Molinàs-Mata*
Max-Planck-Institut für Festkörperforschung, Heisenbergstrasse 1, D-70569 Stuttgart, Federal Republic of Germany
(Received 24 November 1993)

A description of the surface structures consisting of hexagonal (2×2)-reconstructed domains of adatoms, which tile the (111) face of diamondlike crystals and have domain boundaries building up a continuous net of $c(4\times2)$-antiphase domain boundaries, is presented. Calculations of the structure factors of such honeycomb reconstructions show that not all of them account for the splitting of the half-order reflections observed in the diffraction pattern of the moderate-temperature phase of Ge(111). The relation between the splitting and the average domain radius of the honeycomb structures is deduced. Using the temperature dependence of the splitting measured by Phaneuf and Webb [Surf. Sci. **164**, 167 (1985)], the average domain radius is found to vary almost linearly with temperature. The effect on the diffraction pattern of either the deformation compatible with a perfect honeycomb net of antiphase domain boundaries or the breaking of this net is discussed. Deformed structures are similar to those real-space images obtained with the scanning tunneling microscope on the stabilization at room temperature of the moderate-temperature phase of Ge(111) by means of Ga.

I. INTRODUCTION

In the past, a huge body of literature has dealt with the study of the effect of antiphase domain boundaries (ADB's) on the structural[1,2] and the electronic properties[3] of bulk materials and surfaces. An ADB can arise for two reasons: the interchange of the chemical species which occupy equivalent sublattices of the crystal or the breaking of the periodicity of the structure accompanied by no atomic substitutions. Typical examples of these ADB's are found in bulk Au_3Cu (Refs. 1, 4, and 5) and in Pt_3V (Refs. 6 and 7) for substitutional and structural disorder, respectively. In this work we focus on the latter type of ADB's for the particular case of the (111) surfaces in crystals with the diamond structure. It is well known that ADB's occur in both reconstructed clean surfaces (Ge(111)-$c(2\times8)$ (Ref. 8)) as well as on chemisorbed (Ni(111)-O (Ref. 9)) and physisorbed (Kr on graphite[10–12]) surfaces. The necessary condition for the formation of ADB's on a surface is the existence of more than one equivalent domain of the reconstruction on top of the truncated bulk. The spatial origins between those equivalent domains are separated by a multiple of the lattice vectors of the unrelaxed surface, which is a submultiple of the lattice vectors of the reconstructed surface.

The indicative feature in the diffraction spectra of the presence of ADB's in a surface is the splitting or broadening of those reflections[5] which arise from the breaking of the periodicity inside the domains by the ADB's. In this paper, we examine the origin of the splitting of the half-order reflections of the moderate temperature (MT) (between ~ 300 °C and ~775 °C) Ge(111) surface and its relation to the presence of ADB's on the surface. In order to achieve a consistent description of the low-energy electron-diffraction (LEED) pattern of both the MT phase of Ge(111) (Ref. 13) and its stabilization at room temperature (RT),[14–18] structure-factor calculations of honeycomb reconstructions, which are built up with regular and irregular hexagonal (2×2)-reconstructed domains, have been performed. The interest in these structures arises from the model proposed by Phaneuf and Webb in order to explain the diffraction pattern of the MT phase of Ge(111).[13] The same diffraction pattern, characterized by split reflections at half-order sites, was observed, in fact, at room temperature on Ge(111)/Al,[14] Ge(111)/In,[15,16] and Ge(111)/Ga surfaces,[17,18] leading to the conclusion that the structure of the impurity-stabilized phase should resemble the MT phase at least on a time scale corresponding to the diffraction experiment. Feenstra *et al.* reported on the high mobility of the adatoms above 300 °C, which hinders one from obtaining an atomically resolved image of the surface with the scanning tunneling microscope (STM).[19–21] The presence of well-defined reflections in the LEED pattern above 300 °C indicates that the adatoms do sit at discrete positions on the surface (T_4 sites) and still account for the bonding proper of the $c(2\times8)$-reconstructed surface in photoelectron diffraction.[22] Indeed Patthey *et al.* found with this technique that the bonding of the MT phase was equivalent to that of the $c(2\times8)$ reconstruction.[22] Therefore, the MT phase should be only a reordering of the $c(4\times2)$- and (2×2)-building blocks of the $c(2\times8)$ structure.

As a possible model for the MT phase, Phaneuf and Webb suggested that this surface could be tiled by the repetition of a (2×2)-reconstructed regular hexagon of adatoms sitting at T_4 positions. They also considered, however, those nonperiodic structures having the same average domain size as that already mentioned. Recent STM images[17,18] obtained on the Ga-stabilized MT phase of Ge(111) showed also (2×2)-reconstructed hexagonal domains of adatoms, sitting at T_4 positions. The observed adatom pattern, formed by regular and irregular hexagons, does not stay in contradiction with Phaneuf and Webb's model. However, the exact origin and

0163-1829/94/49(24)/17149(11)/$06.00 ©1994 The American Physical Society

dependence of the average size of the hexagons and the observed splitting remains unsolved. Moreover, it is not clear that the diffraction pattern of *any* honeycomb structure with an arbitrary average domain size will reproduce the expected diffraction pattern of the MT phase, in which the only observed reflections are transversally split spots at the half-order positions. Our interest in performing the present calculations is to examine, as already proposed by Phaneuf and Webb,[23] to what extent the $I(2\times2)$-structure corresponds to the MT phase of the Ge(111) surface.

A honeycomb domain structure can be characterized by the average domain size of the building block hexagons. A parameter, the average domain radius of the hexagon ($\overline{R_D}$), will be introduced in order to describe each such structure. We shall show that the two kinds of structures proposed by Phaneuf and Webb [with the somewhat misleading name of incommensurate (2×2) ($I(2\times2)$) structures][13] correspond to a very restrictive sort of (2×2)-reconstructed domains of adatoms with the topology of a honeycomb, namely, those with odd domain radius (R_D) or, if disordered or deformed (see below), with an odd $\overline{R_D}$. The $I(2\times2)$ structures (the notation is maintained for the sake of clarity) have odd R_D, and, therefore, correspond to what we will call in this work class $\langle 1\rangle$ structures. A deformation which preserves the honeycomb structure should keep invariant both the total length of the $c(4\times2)$ ADB's parallel to the three equivalent triagonal directions and the number of $(\sqrt{3}\times\sqrt{3})$ crossings,[24–26] since, otherwise, the deformation induces discontinuities (voids) in the net of $c(4\times2)$-ADB's. These two types of structures arising from deformation of the periodic ones will be called here disordered and deformed, respectively.

The outline of the manuscript is as follows. After a description in Sec. II of the different sorts of honeycomb (2×2)-reconstructed surfaces and the nomenclature used throughout the paper for these structures, we present in Sec. III the calculations of the structure factors at the half-order positions. From these calculations, the relation between the two splittings of the half-order reflections, longitudinal and transverse, and the average domain radius will be deduced. Sections IV and V are devoted, respectively, to the origin of both splittings and to the effect of short-range disorder on the diffraction pattern. In Sec. VI we analyze the temperature dependence of the transverse splitting on the MT phase of Ge(111) (Ref. 13) using the dependence of the transverse splitting on the average domain radius obtained in Sec. III. The variation of the average domain radius with temperature is found to be almost linear. We suggest that the MT phase of Ge(111) could be a commensurate-incommensurate phase transition in Sec. VII, where the results are summarized and the conclusions presented.

II. HONEYCOMB (2×2)-RECONSTRUCTED DOMAIN STRUCTURES

Three types of honeycomb structures will be discussed in this work: periodic, disordered, and deformed. The periodic honeycomb structures show threefold symmetry and can be further classified depending on the number of hexagons within the unit cell. The simplest kind of periodic honeycomb (2×2)-reconstructed domain structures, already proposed by Phaneuf and Webb in 1985,[13] are those built up by the repetition of a single hexagon. One such structure is shown in Fig. 1. We define the domain radius (R_D) of such a honeycomb structure as the distance in (1×1)-surface lattice units between the center of the regular hexagon and the center of the half $(\sqrt{3}\times\sqrt{3})$ unit cell at the edge of the regular hexagon as indicated in Fig. 1. Due to the fact that the hexagon is regular, this distance is the same as the length of each edge of the building hexagon as illustrated in Fig. 1. The relation between the R_D, and the number of adatoms sitting along the antiphase domain boundary at the edge of each hexagon, n, is given by

$$R_D = 2n - 1 . \tag{1}$$

In the structure of Fig. 1 the $c(4\times2)$-reconstructed domain boundaries are formed by two rows of three adatoms each (n=3) and the domain radius corresponds to $5\times(1\times1)$-surface lattice units. The honeycomb structures formed by repetition of only one hexagon have necessarily an odd R_D. We refer to this group of structures as class $\langle 1\rangle$ structures because their R_D's are given by $1+2j$, where $j \in \mathbb{N}$ $(j > 0)$.

For R_D's, which are not odd numbers, the surface cannot be tiled solely with one regular hexagon. The unit cell of the threefold symmetric reconstruction includes a few hexagons, some of them irregular (see Fig. 2). We wish to establish a correspondence between the structures with rational (not odd) domain radius and those with odd domain radius. The number of hexagons inside the unit cell depends on the relative "unmatching"

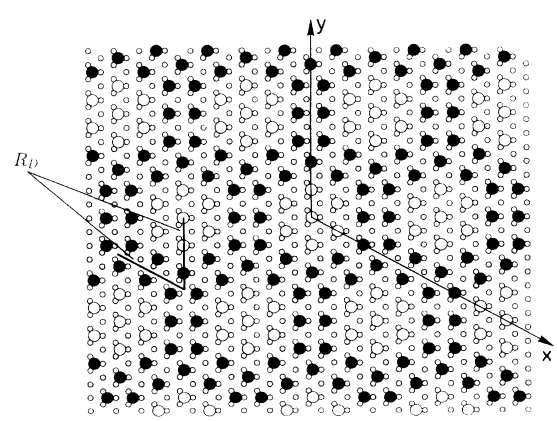

FIG. 1. Periodic honeycomb structure of (2×2)-reconstructed domains of adatoms on a diamondlike (111) surface. Large circles correspond to adatoms at T_4 positions either inside the domains (unfilled) or at the antiphase domain walls (filled). Small circles show the underlying hexagonal (1×1) mesh of the unreconstructed (111) surface. The R_D of this structure is five times larger than the (1×1)-lattice-unit length ($5\times a_{0[1\bar{1}0]}$, $a_{0[1\bar{1}0]}$= 4 Å in Ge). For structures with odd domain radii (class $\langle 1\rangle$ structures) the unit cell contains a single regular hexagon (χ=1).

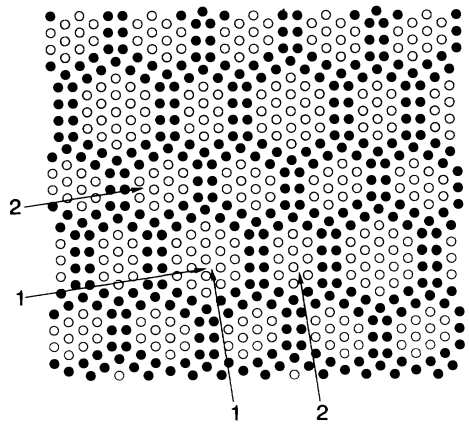

FIG. 2. Periodic honeycomb structure with even average domain radius (class $\langle 0 \rangle$) ($\overline{R_D}$=6). Circles represent adatoms at T_4 positions either inside the domains (unfilled) or at the antiphase domain walls (filled). In case of an even domain radius the unit cell of the structure includes one regular and three irregular hexagons (χ=2^2). A unit cell is indicated by enumerating the two domains along its two inequivalent sides.

of the honeycomb structure (with rational R_D) to that of a structure built up by a single hexagon (with odd R_D). We quantify the degree of "matching" of a structure of arbitrary R_D with respect to that of a structure with odd R_D using the number of hexagons inside the unit cell of the structure, χ, as a parameter. When χ equals 1, the structure is built up by repetition of solely one regular hexagon. The lower the matching, the higher χ. For example, χ=2^2 for even R_D (Fig. 2), χ=4^2 for $R_D = 0.5 + 2j$ (Fig. 3), and χ=10^2 in case of structures with $R_D = 0.8 + 2j$ (Fig. 4). $\chi \to \infty$ corresponds to a structure with irrational domain radius ($R_D \in \mathbb{I}$), a strictly speaking incommensurate structure.[27] Due to the fact that no domain radius can be defined when R_D is not odd (the unit

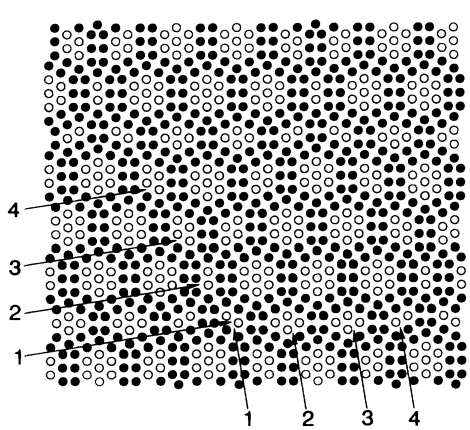

FIG. 3. Periodic honeycomb structure belonging to class $\langle 0.5 \rangle$ ($\overline{R_D}$=4.5). Circles represent adatoms at T_4 positions either inside the domains (unfilled) or at the antiphase domain walls (filled). Sixteen hexagonal domains form the unit cell of the reconstruction (χ=4^2). As in Fig. 2 the unit cell is indicated by enumerating the domains along its two inequivalent sides.

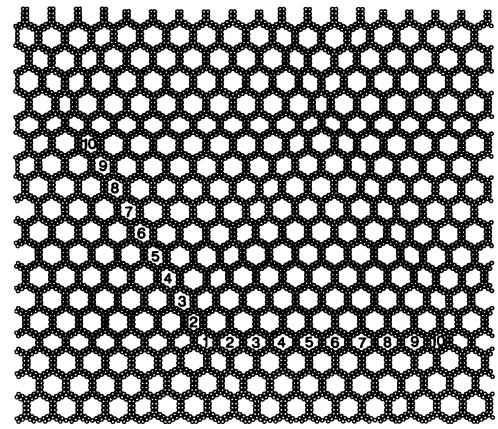

FIG. 4. Periodic honeycomb structure belonging to class $\langle 0.8 \rangle$ ($\overline{R_D}$=6.8). Circles represent adatoms at the antiphase domain walls. Those adatoms inside the domains have not been plotted for the sake of clarity. One hundred hexagonal domains form the unit cell of the reconstruction (χ=10^2). A unit cell is indicated in the same fashion as in Figs. 2 and 3.

cell does not contain a single regular hexagon), R_D shall be substituted by average domain radius ($\overline{R_D}$), which, in fact, accounts for the resulting distribution in size of the different hexagons. With not odd R_D, the unit cell of the reconstruction is tiled by regular and irregular hexagons, whose average domain radius is $\overline{R_D}$. Each rational number q ($0 \leq q < 2$) defines a class of structures, $\langle q \rangle$, whose $\overline{R_D}$ are given by

$$\overline{R_D} = q + 2j\,, \tag{2}$$

where $j \in \mathrm{N}$ (j>0).

The second and third groups of structures we will deal with are not periodic and do not show threefold symmetry. We produce them by deformation of the periodicity of the $c(4\times2)$-reconstructed net of antiphase domain walls of the periodic honeycomb structures. Two kinds of deformations will be discussed. The deformation leading to disordered structures like that in Fig. 5 consists

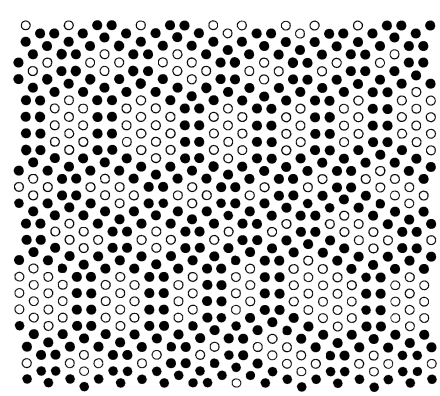

FIG. 5. Disordered honeycomb structure with odd domain radius (class $\langle 1 \rangle$) ($\overline{R_D}$=5). Circles represent adatoms at T_4 positions either inside the domains (unfilled) or at the antiphase domain walls (filled). The deformation shown is compatible with the $c(4\times2)$-reconstructed net of antiphase domain walls.

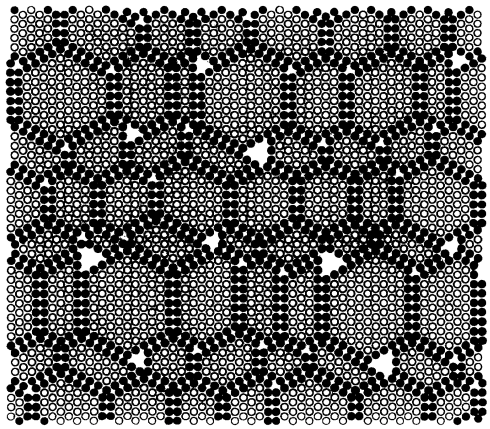

FIG. 6. Deformed honeycomb structure with $\overline{R_D}$=7.6 (class $\langle 1.6 \rangle$). In contrast to the disordered structure in Fig. 5, the continuous $c(4\times2)$-reconstructed net of ADB's shows voids of various sizes at crossings of ADB's. Circles represent adatoms at T_4 positions either inside the domains (unfilled) or at the antiphase domain walls (filled).

of changing the shape of the hexagonal (2×2) domains, while the continuity of the net of $c(4\times2)$-reconstructed domain walls is preserved. In these disordered structures, the crossings between domain walls represent, exactly like in the case of periodic structures, half $(\sqrt{3}\times\sqrt{3})$ unit cells. The $\overline{R_D}$ is kept constant all over the surface so that long-range order remains after deformation. The fluctuations of the domain radius from the average value $(\overline{R_D})$, however, are larger than in the periodic structures because these deformations are random though constrained to respect the continuity of the $c(4\times2)$ net. Under this first class of deformations both the total length of the antiphase domain boundaries along each of the three equivalent directions on the surface and the total number of domain-wall crossings remain constant. This degeneracy [many structures are possible under the constraint of a fixed total length for the $c(4\times2)$ ADB's and a fixed number of $(\sqrt{3}\times\sqrt{3})$ crossings] is not a particular fact of (2×2)-reconstructed domain structures. In fact, the honeycomb $(\sqrt{3}\times\sqrt{3})$-reconstructed domain structures observed in some physisorbed systems[24–26,28–32] show, also, structural degeneracy, which has an associated nonvanishing configurational entropy.[33]

The third type of structures, the deformed, are obtained by further deformation of the $c(4\times2)$ net of domain walls, which leads to topological defects, whose winding number is the same as that of the perfect tiling.[34] The constraint that antiphase domain walls intersect always forming half $(\sqrt{3}\times\sqrt{3})$-reconstructed arrangements of adatoms is relaxed. Therefore, the presence of voids at the place of some otherwise $(\sqrt{3}\times\sqrt{3})$-reconstructed crossings of domain walls is characteristic of these structures as shown in Fig. 6.

III. THE SPLITTINGS OF THE HALF-ORDER REFLECTIONS

In this section we deduce the magnitude of both the longitudinal and transverse splittings of the half-order reflections (see Fig. 7) as a function of the $\overline{R_D}$. Therefore, we calculate the structure factors $(S(\vec{k}))$ at the half-order reflections along both the $(1,0)$ direction and perpendicular to it through the $(\frac{1}{2},0)$ point as labeled by longitudinal and transverse, respectively, in Fig. 7. We define the structure factor, $S(\vec{k})$, as

$$S(\vec{k}) = |\rho(\vec{k})|^2 \ , \ \rho(\vec{k}) = \sum_{j=1}^{N} e^{i\vec{k}\cdot\vec{r_j}} \ , \qquad (3)$$

where N and $\vec{r_j}$ are, respectively, the total number of atoms and their positions. For the sake of clarity in plots of structure factor versus $\vec{k}$ vector we divide $S(\vec{k})$ by N, thus, the intensity of the (0,0) reflection is normalized to 1. Only the overlayer of adatoms was taken into account in the calculation because no significant differences concerning position and intensity of the split reflections were found in the diffraction spectrum when including the first underlying (1×1) layer of atoms.

The honeycomb reconstructions belonging to class $\langle 1 \rangle$ are built up by a single regular hexagon (χ=1) like that in Fig. 1. Their diffraction patterns show splitting of the half-order reflections both along the $(1,0)$ direction (longitudinal splitting) and perpendicular to it (transverse splitting) as depicted in Fig. 8. Whereas the distance between the longitudinally split reflections does not follow a definite trend with increasing R_D, the transverse splitting decreases monotonously with increasing R_D. Exactly like class $\langle 1 \rangle$ structures, those belonging to class $\langle 0 \rangle$ ($\chi=2^2$) are characterized by a monotonic decrease of the transverse splitting with increasing domain size, while the intensities remain constant at approximately 0.5 (see Fig. 9). Along the (1,0) direction, however, we find a qualitative difference with the diffraction spectra of class $\langle 1 \rangle$ structures: the reflection at $(\frac{1}{2}$,0) appears for the five investigated structures. The intensity of this reflection decreases with increasing domain radius. In addition we notice the presence of longitudinal split reflections in two of the five structures of class $\langle 0 \rangle$. Only along the direction perpendicular to the $(1,0)$ direction,

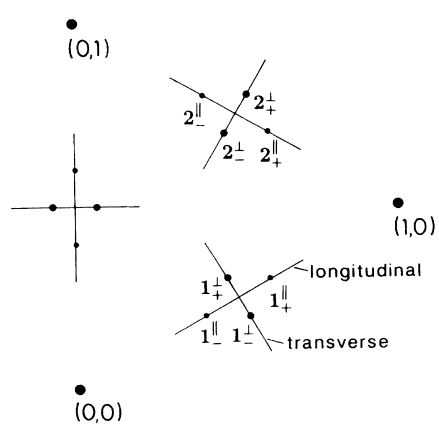

FIG. 7. Scheme of the split spots for a honeycomb (2×2)-domain structure with odd $\overline{R_D}$. The positions of the split spots correspond to those of such a structure with an average domain radius $(\overline{R_D})$ of 5 (see Table I).

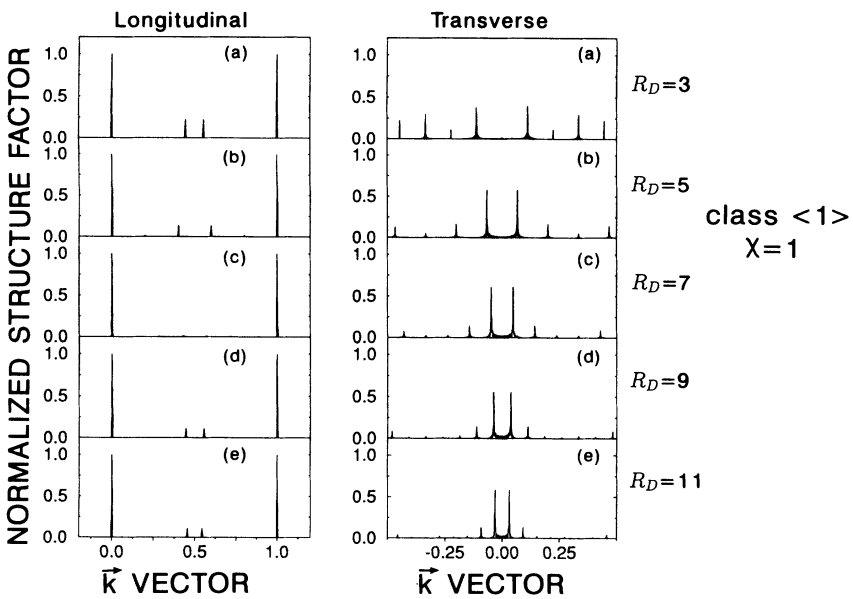

FIG. 8. Calculated structure factors along the (1,0) direction (left) and perpendicular to it through the ($\frac{1}{2}$,0) point of 5 (2×2)-honeycomb structures belonging to class ⟨1⟩ (χ=1). R_D = 3 (a), 5 (b), 7 (c), 9 (d), and 11 (e). The left side shows that $\vec{k}$ is the reciprocal vector along the longitudinal direction indicated in Fig. 7. The right side shows that $\vec{k}$ is the projection along (0,1) of the reciprocal vector parallel to the transverse direction in Fig. 7.

we do observe split half-order reflections for the class ⟨0.5⟩ structures (χ=4^2) in Fig. 10. Their normalized intensities correspond to those observed in class ⟨1⟩ and ⟨0⟩ structures, approximately 0.5. In contrast to the calculations for class ⟨1⟩ and ⟨0⟩ structures, no longitudinal splitting occurs for those belonging to class ⟨0.5⟩. Instead the calculation predicts a weak reflection at the ($\frac{1}{2}$,0) position. For structures with larger χ the structure factor along the (1,0) direction is almost featureless. In order to illustrate this, we show in Fig. 11 the diffraction pattern for three such structures: $\overline{R_D}$=6.8 (χ=10^2), $\overline{R_D}$=7.6 (χ=10^2), and $\overline{R_D}$=8.75 (χ=8^2). The lack of intense reflections along the (1,0) direction and the permanence of the transverse splitting with intensities comparable with those for class ⟨0⟩, ⟨1⟩, and ⟨0.5⟩ structures are common features of honeycomb reconstructions with large χ.

In order to clarify whether the decrease of the transverse splitting with increasing $\overline{R_D}$ follows a common law for structures belonging to different classes, we plot in Fig. 12 the component of the transverse splitting along the (0,1) direction (we call this projection P_S) as a function of the $\overline{R_D}$. All the calculated split reflections, independent of the class to which they belong, fit along the hyperbola:

$$P_S = \frac{1}{3\overline{R_D}} \quad . \tag{4}$$

Similarly, the magnitude of the longitudinal splitting is fixed exclusively by the $\overline{R_D}$ of the structure.

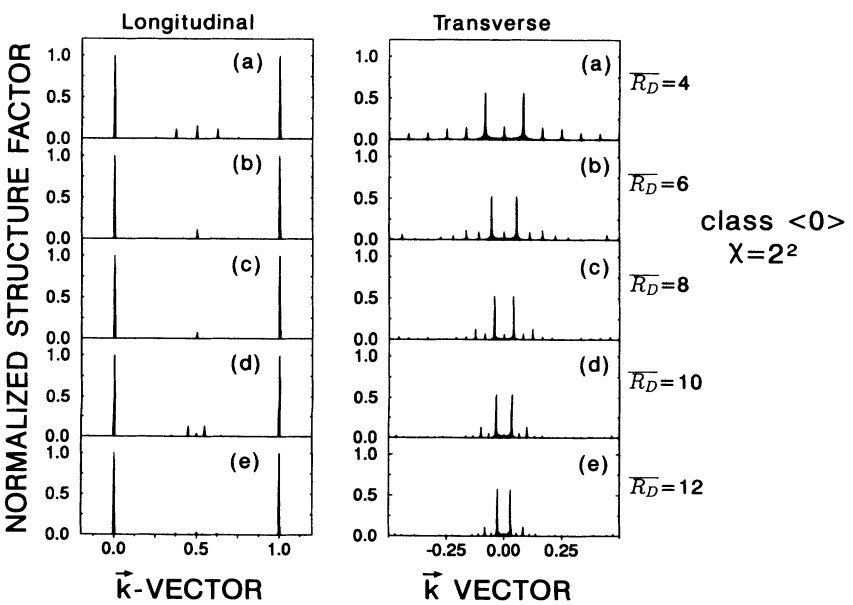

FIG. 9. Calculated structure factors along the (1,0) direction (left) and perpendicular to it through the ($\frac{1}{2}$,0) point of 5 (2×2)-honeycomb structures belonging to class ⟨0⟩ (χ=2^2). $\overline{R_D}$ = 4 (a), 6 (b), 8 (c), 10 (d), and 12 (e). $\vec{k}$ is the same as in Fig. 8.

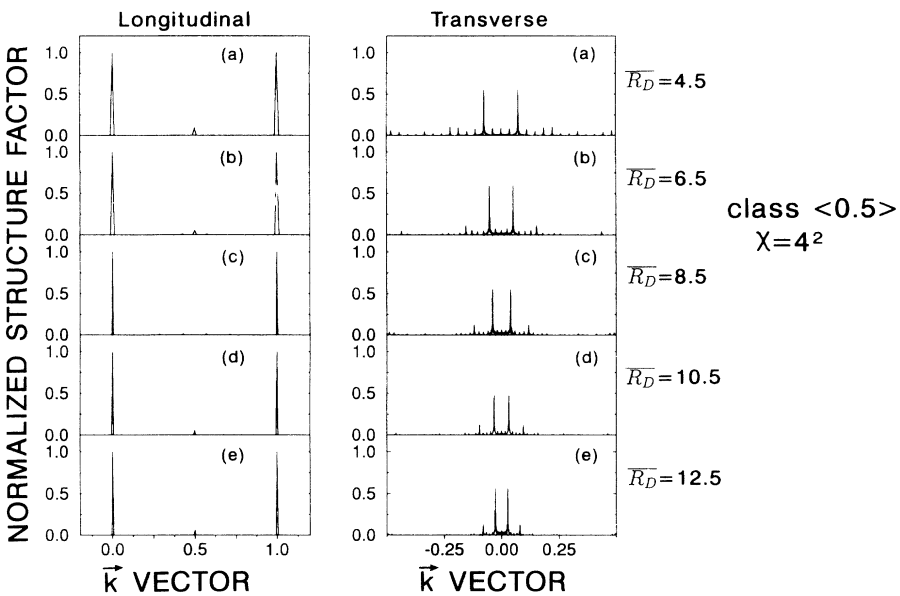

FIG. 10. Calculated structure factors along the (1,0) direction (left) and perpendicular to it through the ($\frac{1}{2}$,0) point of 5 (2×2)-honeycomb structures belonging to class ⟨0.5⟩ (χ=4^2). $\overline{R_D}$ = 4.5 (a), 6.5 (b), 8.5 (c), 10.5 (d), and 12.5 (e). $\vec{k}$ is the same as in Fig. 8.

IV. THE ORIGIN OF THE SPLIT REFLECTIONS AT ($\frac{1}{2}$,0) POINTS

How can we understand the dependence of the transverse and longitudinal splittings on the $\overline{R_D}$? Next, based on the fact that structures with odd domain radius exhibit both types of splittings, we infer their origin in such a structure and, with the information gained, justify why the longitudinal splitting progressively disappears with increasing χ. The relationship between the two sorts of splittings and the $\overline{R_D}$ arises from the fact that the periodicity along (perpendicular to) the ADB is responsible for the transverse (longitudinal) splitting.

We can associate with each vector in reciprocal space, $\vec{k}$, a periodicity, i.e., a wavelength, $\lambda = ||\vec{a_1}' + \vec{a_2}'||$ along the corresponding direction of $\vec{k}$ in real space. $\vec{a_1}'$ and $\vec{a_2}'$ are vectors parallel to the $(\vec{1},0)$ and $(0,\vec{1})$ directions, respectively. An interference maximum in reciprocal space (a reflection) occurs at $\vec{k}$ when a large number of atoms stay in phase with a wave having the corresponding wavelength and direction. This means that a multiple of the period $\vec{a_1}' + \vec{a_2}'$ should equal the distance between equivalent positions in the structure. In case of an infinite (2×2)-reconstructed domain, the periodicity in real space responsible for interference maxima in reciprocal space will be given by the vectors $\vec{a_1}'=(2,0)$ and $\vec{a_2}'=(0,2)$ or linear combinations thereof. By the introduction of ADB's and therefore by breaking the symmetry of the infinite (2×2) domain, $\vec{a_1}=(2,0)$ and $\vec{a_2}=(0,2)$ are no longer those vectors in real space whose linear combinations correspond to the distances between equivalent positions (for example, domain centers) in neighboring domains.

A. Transverse splitting

The distance between the centers of two neighboring domains along the ADB's is given by $(3R_D, 3R_D)$. Therefore no multiple of $(2,2)$ can connect equivalent positions of domains along the ADB's. The periodicity $\vec{a_1}' + \vec{a_2}'$ along the ADB's should be shorter (Fig. 13) or larger (Fig. 14) than that of $(2,2)$ in order to correspond to

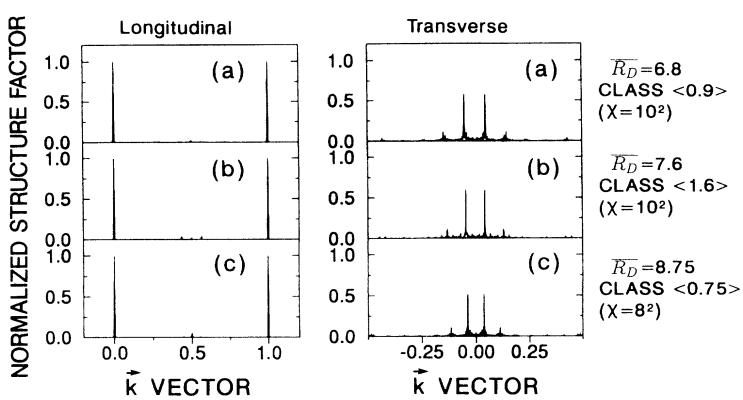

FIG. 11. Calculated structure factors along the (1,0) direction (left) and perpendicular to it through the ($\frac{1}{2}$,0) point of three (2×2)-honeycomb structures belonging to ⟨0.8⟩ ($\overline{R_D}$=6.8, χ=10^2), ⟨1.6⟩ ($\overline{R_D}$=7.6, χ=10^2), and ⟨0.75⟩ ($\overline{R_D}$=8.75, χ=8^2) classes. $\vec{k}$ is the same as in Fig. 8.

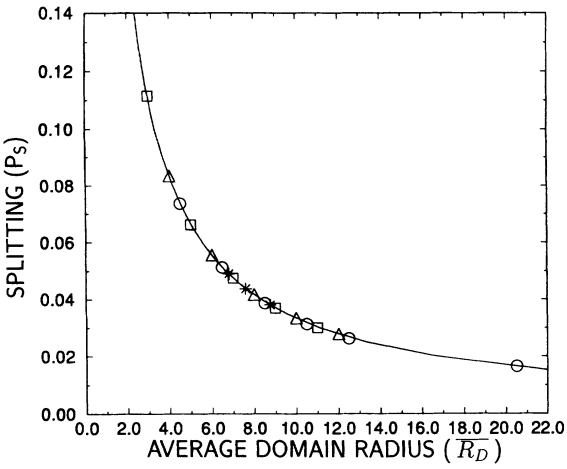

FIG. 12. Dependence of the splitting (P_S) on the R_D for some honeycomb structures, whose $\overline{R_D}$'s belong to different classes. Triangles, circles, and cubes correspond to class $\langle 0 \rangle$ (χ=2^2), $\langle 0.5 \rangle$ (χ=4^2), and $\langle 1 \rangle$ (χ=1) structures, respectively, whereas stars account for structures belonging to other classes: $\langle 0.8 \rangle$ ($\overline{R_D}$=6.8, χ=10^2), $\langle 1.6 \rangle$ ($\overline{R_D}$=7.6, χ=10^2), and $\langle 0.75 \rangle$ ($\overline{R_D}$=8.75, χ=8^2).

a constructive interference. Assuming that the periodicity equals $(2,2)$ multiplied by a rational factor p, the in-phase condition is

$$p\,(3R_D \pm 1)\,(2,2) = 3\,R_D\,(2,2)\ . \tag{5}$$

With the determination of the factor p,

$$p = \frac{3R_D}{3R_D \pm 1}\ , \tag{6}$$

$\vec{a_1}' + \vec{a_2}'$ corresponds to the periodicities in real space $(2\frac{3R_D}{3R_D+1}, 2\frac{3R_D}{3R_D+1})$ and $(2\frac{3R_D}{3R_D-1}, 2\frac{3R_D}{3R_D-1})$. The inverses of the periodicities found, the positions of the reflections

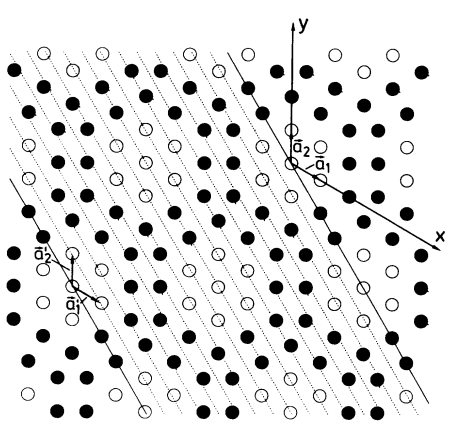

FIG. 13. Honeycomb structure with odd domain radius (R_D=5). The distance between nearest-neighbor dashed lines represents a periodicity parallel to $(2,2)$, which guarantees the in-phase condition along the ADB's between the adatoms of different domains. The plotted periodicity, whose modulus is shorter than that of $(2,2)$, corresponds to the $2^{\perp}_{+}$ reflection in Fig. 7 and Table I.

TABLE I. Splitting of the half-order reflections along the longitudinal and transverse directions shown in Fig. 7. For the longitudinal and transverse splittings, (k_x,k_y) are the components of the projected $\vec{k}$ vectors along the hexagonal (1,0) and (0,1) directions, respectively.

Longitudinal splitting		Transverse splitting	
Reflection	(k_x, k_y)	Reflection	(k_x, k_y)
$1^{\parallel}_{+}$	$(\frac{1}{2}\frac{R_D+1}{R_D},0)$	$1^{\perp}_{+}$	$(\frac{1}{2}\frac{3R_D-1}{3R_D},\frac{1}{3R_D})$
$1^{\parallel}_{-}$	$(\frac{1}{2}\frac{R_D-1}{R_D},0)$	$1^{\perp}_{-}$	$(\frac{1}{2}\frac{3R_D+1}{3R_D},\frac{-1}{3R_D})$
$2^{\parallel}_{+}$	$(\frac{1}{2}\frac{R_D+1}{R_D},\frac{1}{2}\frac{R_D-1}{R_D})$	$2^{\perp}_{+}$	$(\frac{1}{2}\frac{3R_D+1}{3R_D},\frac{1}{2}\frac{3R_D+1}{3R_D})$
$2^{\parallel}_{-}$	$(\frac{1}{2}\frac{R_D-1}{R_D},\frac{1}{2}\frac{R_D+1}{R_D})$	$2^{\perp}_{-}$	$(\frac{1}{2}\frac{3R_D-1}{3R_D},\frac{1}{2}\frac{3R_D-1}{3R_D})$

$2^{\perp}_{+}$ and $2^{\perp}_{-}$ in Fig. 7, are given in Table I. With similar arguments one can deduce the periods: $(2\frac{3R_D}{3R_D-1}, +3R_D)$ and $(2\frac{3R_D}{3R_D+1}, -3R_D)$, whose inverse values correspond to the $1^{\perp}_{+}$ and $1^{\perp}_{-}$ reflections in Fig. 7.

B. Longitudinal splitting

In order to fulfill the in-phase condition along the direction perpendicular to the ADB's (see Fig. 15), the p factor should be a solution of the following in-phase equation:

$$p\,\frac{R_D \pm 1}{2}\,(2,0) = R_D\,(2,0)\ . \tag{7}$$

The so obtained periodicities are $\vec{a_1}' = (\frac{2R_D}{R_D+1},0)$ and $\vec{a_1}' = (\frac{2R_D}{R_D-1},0)$. Their inverses, presented in Table I, correspond to the reflections $1^{\parallel}_{+}$ and $1^{\parallel}_{-}$ in Fig. 7.

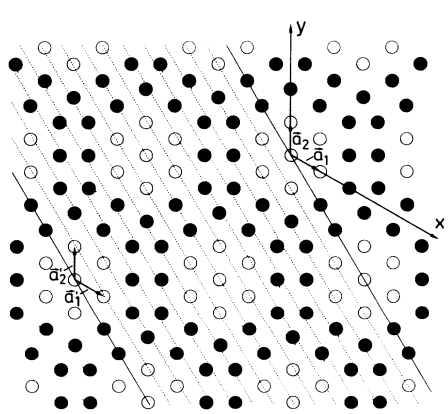

FIG. 14. The same structure as in Fig. 13. The indicated periodicity, of larger modulus than that of the vector $(2,2)$, corresponds to the $2^{\perp}_{-}$ reflection in Fig. 7 and Table I.

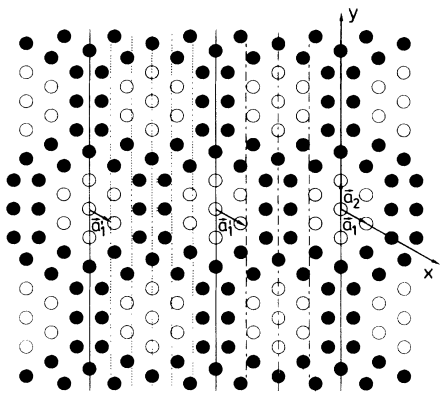

FIG. 15. The same structure as in Fig. 13. The distance between nearest-neighbor dashed lines represents a periodicity parallel to $(2,0)$, which guarantees the in-phase condition perpendicularly to the ADB's. Their moduli, shorter (left) or larger (right) than the projection of vector $(2,0)$, correspond to the $1^{\parallel}_{+}$- and $1^{\parallel}_{-}$ reflections in Fig. 7 and Table I, respectively.

C. Spot splitting for structures with large χ

In case of honeycomb structures which present a large "unmatching" ($\chi \gg 1$) with those of class $\langle 1 \rangle$, the normalized intensity of the transversally split half-order reflections lies around 0.5 (see for example Fig. 11), exactly as it does for class $\langle 1 \rangle$ and $\langle 0 \rangle$ structures. Therefore, the in-phase condition for the tranverse splitting is still fulfilled. On the other hand the number of atoms which contribute to constructive interference along the direction perpendicular to the ADB's decreases as χ increases because of the increasing dispersion in the position of the ADB's projected to the direction perpendicular to them as indicated in Fig. 16 for the periodic honeycomb structure with $\overline{R_D} = 7.6$. Indeed the ADB's line up in class $\langle 1 \rangle$ structures so that a periodicity exists perpendicular to them. The longitudinal reflections, either split or at $(\frac{1}{2},0)$, do not sharply disappear above a particular χ value, but their intensity progressively disminishes with increasing χ. As we will discuss in the next section, short-range disorder, either compatible or not with the $c(4\times2)$ net of ADB's, accounts for an additional supression of the intensity of the longitudinal split reflections.

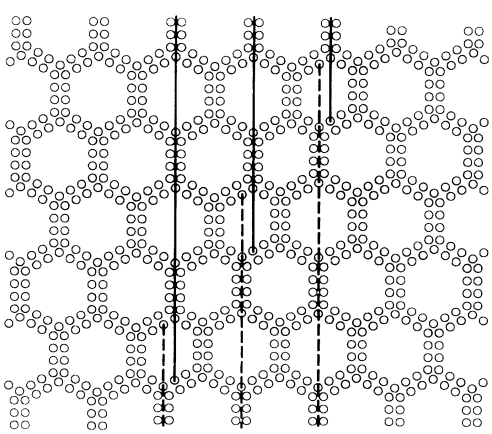

FIG. 16. Periodic honeycomb structure ($\overline{R_D}$=7.6) with large χ ($\chi = 10^2$); the ADB's do not line up like in $\langle 0 \rangle$-class structures (see Fig. 15). With increasing χ the dispersion in the position along the direction perpendicular to the $\overline{R_D}$'s is responsible for the decrease in intensity of the longitudinal split reflections.

V. THE EFFECT OF SHORT-RANGE DISORDER IN THE SPLIT REFLECTIONS

In order to clarify the influence of deformation of the domain-wall net on the calculated intensities for the half-order split reflections, we compare structure-factor calculations for sets of three structures, namely, periodic, disordered, and deformed structures with the same $\overline{R_D}$. No significant differences exist between those structures showing disorder or deformation. The presence of voids in the deformed structures does not give rise to a large variation in the calculated structure factors of the disordered ones. Therefore we will discuss only the differences between the extreme cases: periodic and deformed. The calculated longitudinal splitting for those structures with $\overline{R_D} = 5$ (χ=1), 6.5 (χ=4^2), and 7.6 (χ=10^2) are shown in Fig. 17. Compared to the periodic structures, no shift in the peak position appears, while the intensity of the reflections decreases slightly. Therefore, for large χ values no longitudinal reflections on deformed honeycomb structures appear.

The effect of deformation on the transverse splitting corresponds to a reduction of the intensity of the reflections as observed in Fig. 18. Additional effects are the spatial localization of the reflections in a smaller segment of the transverse direction and, also, the appearance of small new reflections along it. The deformation of the perfect honeycomb lattice, even when the presence of voids is involved, does not alter the distance between split spots. However, it results in a decrease of the intensity of the split reflections and the appearance of new sharp reflections of much lower intensity along the connecting segment.

VI. THE MODERATE TEMPERATURE PHASE OF Ge(111)

What can be understood about the MT phase of the Ge(111) surface from other measurements using the relationship we have established between the tranverse splitting and the average domain radius? Phaneuf and Webb showed with LEED a monotonic increase of the magnitude of the transverse splitting with temperature from the phase transition up to 900 K.[13] From the relation between transverse splitting and average domain radius ($\overline{R_D}$) in Table I, we infer a decrease of the $\overline{R_D}$ with temperature. Figure 19 accounts for the exact temperature dependence obtained from Phaneuf and Webb's LEED data[13] and the expressions in Table I. The $\overline{R_D}$ decreases linearly with temperature from 7.08–2.81 in the temper-

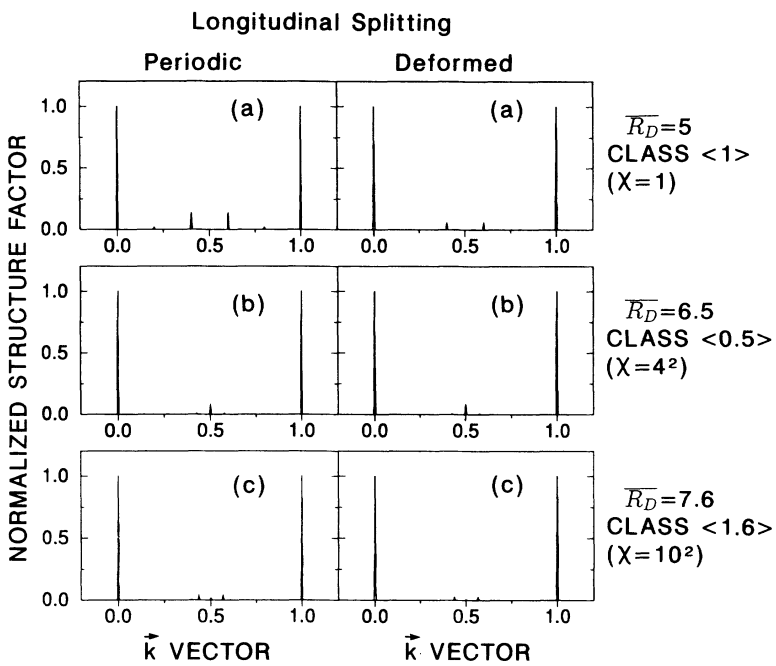

FIG. 17. Calculated longitudinal splitting for the three sets of periodic (left) and deformed (right) structures, corresponding to $\overline{R_D}$ = 5 ($\langle 1 \rangle$, χ=1) (a), 6.5 ($\langle 0.5 \rangle$, χ=4^2) (b), and 7.6 ($\langle 1.6 \rangle$, χ=10^2) (c). The positions of the reflections remain constant after the deformation, whereas the intensity decreases.

ature range 570 K–914 K. Using Eq. (1) the decrease of the $\overline{R_D}$ can be expressed as a decrease of the number of adatoms at the domain edges, n, which varies approximately from 4–2. Disregarding the effect of voids at the surface, the density of adatoms does not remain constant with decreasing $\overline{R_D}$. The relative variation of the density, however, is small:

$$\frac{\rho_{n=2} - \rho_{n=4}}{\rho_{n=2}} = 0.03\,, \tag{8}$$

where $\rho_{n=j}$ stands for the density of adatoms in a $\langle 1 \rangle$ class structure with j atoms at the domain edge. The decrease of the $\overline{R_D}$ supposes an increase of the (4×2)- and ($\sqrt{3}\times\sqrt{3}$)-reconstructed areas relative to those covered with (2×2)-reconstructed cells.

VII. DISCUSSION AND SUMMARY

An overview of the possible tilings of a (111)-truncated surface of diamondlike crystals with hexagonal (2×2)-reconstructed domains of adatoms has been presented. Emphasis was placed on the relation between the average domain size, characterized by the $\overline{R_D}$, and the half-order split reflections. The distance between split reflections along both the longitudinal and transverse directions depends exclusively on the average domain radius. No shift in the position of the reflections appears when introducing disorder, neither compatible with nor breaking the continuity of the honeycomb net of $c(4\times2)$ ADB's. Odd $\overline{R_D}$'s correspond to structures formed by repetition of a single regular hexagon, whose diffraction patterns

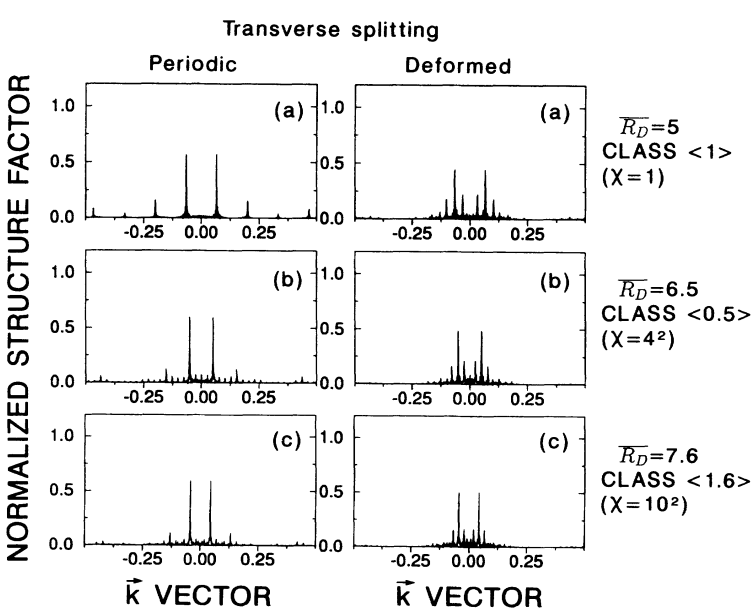

FIG. 18. The same as in Fig. 17 but for the transverse splitting. The intensity of the split half-order reflections (the most intensive) decreases through the deformation. A high number of tiny reflections appear between the split spots.

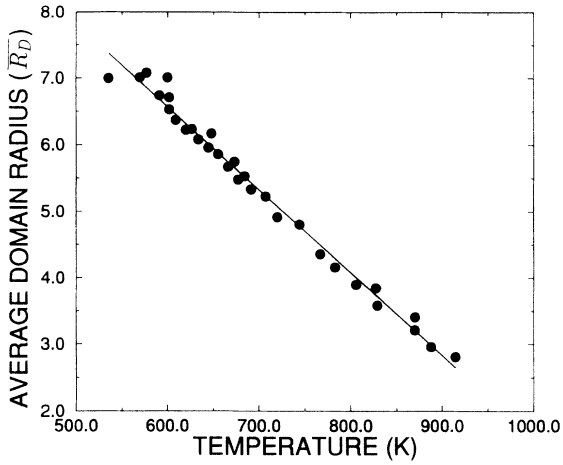

FIG. 19. Temperature dependence of the average domain radius of the honeycomb structures appearing in the moderate-temperature phase of Ge(111). The points were obtained from the temperature dependence of the splitting of the half-order reflections in reciprocal space measured with LEED by Phaneuf and Webb (Ref. 13). Equation (4) was used to express the splitting (P_S) as a function of the $\overline{R_D}$. A line was drawn as a guide for the eye.

show not only transverse splitting, but also a longitudinal one in disagreement with LEED (Ref. 13) and He-diffraction[35] experiments. Deformed $\langle q \rangle$ structures with large χ reproduce the diffraction pattern measured on the MT phase of Ge(111) and on its Ga stabilization at RT; only tranverse split reflections arise from the calculation. Almost no difference appears between the diffraction pattern of a disordered and a deformed honeycomb domain structure with identical $\overline{R_D}$. The reason lies in the fact that the voids introduced in a disordered structure in order to obtain a deformed one represent a set of point defects, whose area is too small to change the diffraction pattern.

The disorder introduced in this work does not account for the broad half-order split reflections measured by Phaneuf and Webb on the MT phase of Ge(111).[13] Stronger fluctuations of the $\overline{R_D}$ all over the surface, as observed with STM on the Ga-stabilized MT phase,[18] would probably lead to a more accurate description of the observed broadening. A realistic modeling, however, would require a deeper knowledge of the long-range structure from STM images and is therefore beyond the scope of this paper.

Taking advantage of the relationship obtained between the magnitude of the splitting and the $\overline{R_D}$, we can reformulate the dependence on temperature of the splitting of the MT phase of Ge(111), which was found with LEED by Phaneuf and Webb,[13] as a dependence of the average domain radius on temperature. The size of the hexagonal domains decreases with temperature. Therefore, independent of the density of voids, the portion of the surface covered by $c(4\times2)$ and $(\sqrt{3}\times\sqrt{3})$ cells increases relative to that (2×2) reconstructed. The tendency to increase the density of adatoms at reconstructed areas when modifying the surface structure is characteristic of commensurate-incommensurate phase transitions observed on physisorbed systems (i.e., Kr on graphite).[24–26,28–32] The honeycomb domain structures in the case of Kr on graphite represent the evolution of the system at the phase transition between a commensurate (C) and an incommensurate (I) structure. On the Ge(111) surface, the MT phase could be also an intermediate state between a C phase [the $c(2\times8)$] and an I phase, whose density should be larger than that of the $c(2\times8)$ ($\frac{1}{4}$ monolayer). Sakamoto and Kanamori performed Monte Carlo calculations of the lattice gas model for the Ge(111) surface.[36] The number of $(\sqrt{3}\times\sqrt{3})$-reconstructed defects increases with temperature in agreement with our results. However, the disorder arising from the lattice gas procedure exceeds the more constrained deformations of the perfect tiling of the surface with (2×2)-reconstructed domains presented here.

A more accurate measurement, for example with surface x-ray diffraction, of the evolution of the split reflections of the MT phase and of the Ga-stabilized one as a function of temperature would be interesting in order to determine to what extent the $\overline{R_D}$ evolves continuously with temperature. The possibility of a devil's staircase behavior[37] like that associated with the 1D anisotropic next nearest neighbor Ising[38,39] model cannot be excluded *a priori*.

ACKNOWLEDGMENTS

I am thankful to R. Feidenhans'l, P.-A. Lindgård, M. Nielsen, and M. Cardona for fruitful discussions and A. Muramatsu for bringing Ref. 34 to my attention. M. Reedyk and D. Leach are gratefully acknowledged for a careful reading of this paper. The Directorate-General for Science, Research and Development of the European Community is acknowledged for partial financial support in this project. I also want to thank the Departament de Física Fonamental de la Universitat de Barcelona and the Institut de Ciència de Materials de Barcelona (CSIC) for hospitality during a part of this project.

* Present address: IBM Research Division, T.J. Watson Research Center, Yorktown Heights, NY 10598.

[1] B.E. Warren, in *X-Ray Diffraction* (Addison-Wesley, Reading, 1969).

[2] M.A. van Hove, W.H. Weinberg, and C.-M. Chang, in *Low-Energy Electron Diffraction* (Springer, Berlin, 1986).

[3] R. Joynt, T.M. Rice, and K. Ueda, Phys. Rev. Lett. **56**, 1412 (1986).

[4] F.W. Jones and G. Sykes, Proc. R. Soc. London Ser. A **166**, 376 (1938).

[5] A. Guinier, in *X-Ray Diffraction* (Freeman, San Francisco, 1963).

[6] J. Planès, A. Loiseau, F. Ducastelle, and G. van Tendeloo, in *Electron Microscopy and Analysis* (Institute of Physics, Bristol, 1988).

[7] F. Ducastelle, in *Order and Phase Stability in Alloys*

(North-Holland, Amsterdam, 1991).
[8] R. Feidenhans'l, J.S. Pedersen, J. Bohr, M. Nielsen, F. Grey, and R.L. Johnson, Phys. Rev. B **38**, 9715 (1988).
[9] L.D. Roelofs, A.R. Kortan, T.L. Einstein, and R.L. Park, Phys. Rev. Lett. **46**, 1465 (1981).
[10] J. Villain and M.B. Gordon, Surf. Sci. **125**, 1 (1993).
[11] S.C. Fain, M.D. Chinn, and R.D. Diehl, Phys. Rev. B **21**, 4170 (1980).
[12] D.E. Moncton, P.W. Stephens, R.J. Birgeneau, P.M. Horn, and G.S. Brown, Phys. Rev. Lett. **46**, 1533 (1981).
[13] R.J. Phaneuf and M.B. Webb, Surf. Sci. **164**, 167 (1985).
[14] W.S. Yang and F. Jona, Solid State Commun. **42**, 49 (1982).
[15] T. Ichikawa and S. Ino, Solid State Commun. **34**, 349 (1980).
[16] M. Böhringer and J. Zegenhagen (unpublished).
[17] P. Molinàs-Mata, J. Zegenhagen, A. Höpner, H. Bender, E. Schönherr, and H. Labitzke, J. Phys. Condens. Matter **5**, 4687 (1993).
[18] P. Molinàs-Mata, M. Böhringer, and J. Zegenhagen, Surf. Sci. (to be published).
[19] R.M. Feenstra, A.J. Slavin, G.A. Held, and M.A. Lutz, Phys. Rev. Lett. **66**, 3257 (1991).
[20] R.M. Feenstra and A.J. Slavin, Surf. Sci. **251**, 401 (1991).
[21] R.M. Feenstra, A.J. Slavin, G.A. Held, and M.A. Lutz, Ultramicroscopy **42**, 33 (1992).
[22] L. Patthey, E.L. Bullock, and K. Hricovini, Surf. Sci. **269**, 28 (1992).
[23] See Ref. 26 in Ref. 13.
[24] J. Villain, in *Ordering in Two Dimensions*, edited by S.K. Sinha (North-Holland, New York, 1980).
[25] J. Villain, Surf. Sci. **97**, 219 (1980).
[26] J. Villain, J. Phys. **41**, L267 (1980).
[27] K. Kern and G. Comsa, in *Chemistry and Physics of Solid Surfaces VII*, edited by R. Vanselow and R. Howe (Springer, Berlin, 1988).
[28] S.N. Coppersmith, D.S. Fisher, B.I. Halperin, P.A. Lee, and W.F. Brinkman, Phys. Rev. Lett. **46**, 549 (1981).
[29] S.N. Coppersmith, D.S. Fisher, B.I. Halperin, P.A. Lee, and W.F. Brinkman, Phys. Rev. B **25**, 349 (1982).
[30] P. Bak, D. Mukamel, J. Villain, and K. Wentowska, Phys. Rev. B **19**, 1610 (1979).
[31] H. Park, E.K. Riedel, and M. den Nijs, Ann. Phys. (N.Y.) **172**, 419 (1986).
[32] R. Kariotis, J.A. Venables, and J.J. Prentis, J. Phys. Condens. Matter **21**, 3031 (1988).
[33] R. Kikuchi, Phys. Rev. B **81**, 988 (1951).
[34] N.D. Mermin, Rev. Mod. Phys. **51**, 591 (1979).
[35] J.S. Ha and E.F. Greene, J. Chem. Phys. **91**, 7957 (1989).
[36] Y. Sakamoto and J. Kanamori, Surf. Sci. **242**, 119 (1991); J. Phys. Soc. Jpn. **58**, 1512 (1989); **58**, 2038 (1989).
[37] P. Bak, Rep. Prog. Phys. **45**, 587 (1982).
[38] M.E. Fisher and W. Selke, Phys. Rev. Lett. **44**, 1502 (1980).
[39] W. Selke and M.E. Fisher, Z. Phys. B **40**, 71 (1980).